Combinatorial effects of multiple genes contribute to beneficial aneuploidy phenotypes

M. Sophie Koller[1,2], Claudia Himmelbauer [1], Sarah Fink[1], Madhwesh C. Ravichandran[1], Christopher S. Campbell[1@]

[1]Department of Chromosome Biology, Max Perutz Labs, University of Vienna, Vienna Biocenter (VBC), A-1030 Vienna, Austria
[2]Vienna Biocenter PhD Program, a Doctoral School of the University of Vienna and the Medical University of Vienna, A-1030 Vienna, Austria

@: Corresponding author
Email: christopher.campbell@univie.ac.at
Phone: +43-1-4277-74418
Address: Dr. Bohr-Gasse 9/5, A-1030 Vienna, Austria

Key words: Aneuploidy; complex karyotypes; drug resistance; tubulin expression;

Abstract

Aneuploidy is one of the most common mechanisms of adaptation to environmental selection in vegetatively growing cells. However, it is still unclear what advantages aneuploidy provides over other types of genomic alterations. In this study, we aimed to determine if beneficial aneuploidy phenotypes are driven primarily by combinatorial expression changes of multiple genes using budding yeast as a model system. To determine the impact of complex aneuploidy on cellular fitness and resistance to a variety of drug treatments, we generated yeast collections with nearly every possible combination of two chromosome gains or losses. In addition, we genetically dissected aneuploid chromosomes using partial deletions to identify chromosomal regions that contribute to aneuploidy-driven drug resistance. Strong resistance phenotypes consistently came from combinations of chromosomes or chromosomal regions. We identified up to five regions on a single chromosome that contribute to resistance to a single drug treatment. Finally, we found that the strongest aneuploidy phenotypes came from synergistic effects between copy number changes of different chromosomes or chromosomal regions. These results provide insights into how combining subtle gene expression changes across the genome impacts aneuploidy phenotypes.

Introduction

The accurate distribution of chromosomes during cell division is essential for maintaining genomic integrity across all eukaryotic species. Chromosome segregation errors result in alterations in chromosome copy number, which are termed aneuploidy. Aneuploidy is one of the most common genetic alterations in cancer, occurring in ~90% of solid tumors and ~70% of hematopoietic cancers (Weaver and Cleveland 2006). These high frequencies of aneuploidy are not only inherent to cancer cells but are also commonly observed within other vegetatively growing cell populations including drug resistant strains of the human pathogen *Candida albicans* and industrial strains of baker's yeast (Selmecki et al. 2006; Peter et al. 2018; Loegler et al. 2024).

Despite the frequency of aneuploidy in mitotically growing cell populations, it is generally associated with reduced cellular fitness. Engineering aneuploidy in cells invariably decreases growth rates under optimal conditions (Torres et al. 2007; Stingele et al. 2012). This decrease in fitness results from changes in gene copy numbers of many transcribed genes on the aneuploid chromosome (Bonney et al. 2015). For both yeast and human cells, gene expression levels of lab engineered aneuploidies scale with gene copy numbers for most of the aneuploid genes (Torres et al. 2007; Stingele et al. 2012; Wangsa et al. 2019; Rojas et al. 2024; Muenzner et al. 2024). These small changes in expression levels for hundreds of genes cause a wide range of deleterious phenotypes. Such general aneuploidy-associated phenotypes include increased proteotoxic stress, cell cycle delays, and increased DNA damage (Torres et al. 2007; Sheltzer et al. 2011; Thorburn et al. 2013; Oromendia et al. 2012; Beach et al. 2017; Li and Zhu 2022).

Yet, aneuploidy is one of the most frequently observed mechanisms of cellular adaptation. The first direct link between adaptive drug resistance and aneuploidy was established in the human pathogen *Candida albicans* (Selmecki et al. 2006). Adaptation via aneuploidy has since been more extensively observed in the budding yeast *Saccharomyces cerevisiae,* where specific aneuploidies consistently emerge during experimental evolution screens under adverse environmental conditions (Gresham et al. 2008; Yona et al. 2012; Chen et al. 2012; Voordeckers et al. 2015; Zhang et al. 2016; Beaupere et al. 2018; Morard et al. 2019). Moreover, inducing

aneuploidy via random chromosome missegregation in both yeast and human cells promotes resistance to a large variety of drugs (Pavelka et al. 2010; Chen et al. 2012; Lukow et al. 2021; Ippolito et al. 2021). Aneuploidy can also act as a suppressor of mutations that decrease cellular fitness (Rancati et al. 2008; Liu et al. 2015; Ryu et al. 2016; Ravichandran et al. 2018; Macaluso et al. 2025). In cancer, karyotype patterns have predictive power for drug resistance, tumor progression and patient outcome (Shukla et al. 2020).

The potential for aneuploidy as an adaptation mechanism to a large variety of selective environments can partially explain the high prevalence of aneuploidy following long-term vegetative growth, such as in cancer or in yeast used for alcohol production (Peter et al. 2018). However, it still fails to explain why cells adapt through aneuploidy over other types of mutations that don't share its inherent downsides. Different models for the specific advantage of adaptation through aneuploidy have been proposed. Aneuploidy has been suggested to be a rapid, but transient solution to sudden environmental changes. In *S. cerevisiae* subjected to acute heat stress, chromosome 3 is gained early in the adaptation process but then lost again over time (Yona et al. 2012). Similarly, yeast adapting to high rates of chromosomal instability (CIN) adapted first through the accumulation of specific aneuploidies, followed later by the accumulation of suppressor point mutations (Clarke et al. 2023). However, there are also many examples of specific aneuploidies that are maintained throughout long-term adaptation, highlighting that speed is likely not the only advantage of adaptation via aneuploidy (Selmecki et al. 2009; Ravichandran et al. 2018; Adell et al. 2023; Clarke et al. 2023; Zhou et al. 2024; Watson et al. 2024).

An additional explanation for the advantages of aneuploidy as a mechanism of adaptation comes from its ability to change gene expression levels of several beneficial genes simultaneously. In yeast adaptation screens, only a handful of examples could attribute the selective advantage of aneuploidy to changes in expression levels of one or two specific genes. Even in these cases, they rarely recapitulated the strength of the aneuploidy phenotype (Selmecki et al. 2009; Chen et al. 2012; Ryu et al. 2016; Linder et al. 2017; Beaupere et al. 2018; Ravichandran et al. 2018; Barney et al. 2021; Pavani et al. 2021; Zhou et al. 2024). In cancer, overexpression of individual genes also fails to fully recapitulate the phenotypes of

86 aneuploid chromosomes (Trakala et al. 2021; Su et al. 2021; Girish et al. 2023). These
87 findings suggest that the challenges of identifying driver genes on aneuploid
88 chromosomes could be amplified by the interplay between multiple genes. It is
89 therefore important to determine if multiple genes acting cooperatively is a general
90 characteristic of aneuploid chromosomes that confer an adaptive advantage.
91
92 In this study, we generated a large yeast collection with nearly every possible
93 combination of two chromosome gains or losses to determine how combinatorial
94 aneuploidy phenotypes impact drug resistance and sensitivity. We found that the
95 strongest resistance phenotypes consistently came from combinations of aneuploid
96 chromosomes, demonstrating the advantage of copy number changes in multiple
97 genes. Additionally, we genetically dissected resistant aneuploid chromosomes using
98 partial arm deletions to determine the number of regions that contribute to aneuploidy-
99 driven drug resistance on a single chromosome. We found that resistance conferred
100 by single disomies nearly always comes from multiple chromosomal regions. While
101 the majority of phenotypes are additive, the strongest resistance phenotypes of
102 aneuploidies came from synergistic effects between different regions or
103 chromosomes.
104

105 **Results**

106 **Generation of yeast strain libraries with combinations of chromosome gains**
107 **and losses**

108 We first determined how aneuploidy of different regions of the genome combine to
109 impact cellular fitness and drug response by generating two collections of yeast with
110 combinations of chromosome gains or losses. The collections consist of nearly all
111 possible single and double chromosome gains and losses (Fig. 1A). To engineer
112 chromosome gain or loss, chromosome-specific missegregation was first induced via
113 a strong galactose-inducible centromere-proximal promotor, followed by selection for
114 the specific aneuploidy (Supplemental Fig. S1A). We selected for chromosome gains
115 via recombination events that restore the function of an auxotrophic marker.
116 Chromosome loss was generated by selecting against the *URA3* gene using 5-
117 fluoroorotic acid (5-FOA) (Supplemental Fig. S1A). The chromosome gain collection

118 includes most of the possible single (14/16) and double disomic (90/136) strains in
119 haploid cells; each was confirmed by qPCR (Supplemental Table S1). The
120 chromosome loss collection contains every possible single or double monosomy in
121 diploid cells (Supplemental Fig. S1B). Since chromosome loss cannot be continuously
122 selected for, this collection is inducible to generate newly aneuploid cells prior to each
123 experiment. These libraries currently constitute the largest collections of engineered
124 complex aneuploid cells.
125
126 We first evaluated the libraries by measuring the growth rates of the engineered
127 aneuploidy strains under optimal growth conditions. Similar to previous observations
128 with single aneuploidies (Beach et al. 2017), the growth of complex aneuploidies
129 scaled with the number of aneuploid open reading frames (ORFs) and chromosome
130 loss is more detrimental to cell growth than chromosome gain (Fig. 1B). Furthermore,
131 the high-throughput growth rate measurements of single disomies and monosomies
132 strongly correlate with those previously observed (Supplemental Fig. S1C). The
133 previously published measurements were performed in a strain background containing
134 a mutation in the *SSD1* gene, which has been reported to sensitize cells to aneuploidy
135 phenotypes (Hose et al. 2020). However, we observe similar results in a different,
136 wildtype *SSD1* background (S288c), indicating that strain background does not
137 substantially alter the relative growth rate of aneuploid yeast.
138
139 We next determined the impact of combining aneuploid chromosomes on cellular
140 fitness. Most of the single and double monosomies are lethal. By contrast, nearly all
141 of the double disomies are viable, with the sole exception of those involving
142 chromosome 6 (Fig. 1B, Supplemental Fig. S1B). To identify potential genetic
143 interactions between aneuploid chromosomes, we calculated growth predictions for
144 all chromosome combinations based on the product of the two single aneuploidies. In
145 general, growth of the double disomies correlates well ($r^2 = 0.64$) with the calculated
146 growth predictions. The strongest outlier is the combination of chromosomes 6 and 13
147 (Fig. 1C). Chromosome 6 disomy is lethal on its own due to the presence of an extra
148 copy of the β-tubulin *TUB2* gene (Anders et al. 2009). However, chromosome 6 disomy
149 becomes viable with the additional gain of chromosome 13. This is consistent with
150 previous observations where selection of chromosome 6 gain resulted in a strain that

151 spontaneously gained the additional disomies of chromosomes 1 and 13 (Torres et al.
152 2007). Chromosome 13 contains the genes for α-tubulin, and overexpression of α-
153 tubulin rescues the lethality of chromosome 6 disomy (Anders et al. 2009). For the
154 chromosome loss collection, the strongest genetic interaction is again between
155 chromosomes 6 and 13 (Fig. 1D). Chromosome 13 monosomy is lethal on its own, but
156 the additional loss of chromosome 6 rescues viability (Fig. 1D). The heterozygous
157 deletion of *TUB2* is sufficient to rescue chromosome 13 monosomy, indicating that
158 excess β-tubulin relative to α-tubulin is the genetic basis behind these strong
159 chromosome copy number interactions (Figure 1D).
160
161 To find additional genetic interactions between chromosome gains, we identified
162 chromosome combinations whose growth significantly differed from the prediction
163 based on single disomies. The data adhered to a normal distribution, enabling the
164 calculation of z-scores (Kolmogorov-Smirnov test). Significant interactions were
165 defined as having z-scores >1 or <-1. Among the 90 chromosome combinations
166 analyzed, we identified 11 positive (12.2%) and 11 negative (12.2%) chromosome
167 copy number interactions (Supplemental Fig. S1D). Importantly, these interactions are
168 substantially stronger than interactions previously demonstrated to heavily impact
169 karyotype pattern formation (Ravichandran et al. 2018). We conclude that, although
170 most combinations of aneuploid chromosomes show additive phenotypes,
171 chromosome copy number interactions are a common feature of aneuploidy
172 combinations.

173 **The strongest drug resistance phenotypes come from strains with multiple**
174 **aneuploid chromosomes**

175 We next used the chromosome gain library to determine if combinatorial interactions
176 between aneuploid chromosomes contribute to improved growth in stress conditions.
177 We measured growth in the presence of four drugs that induce cellular stresses
178 associated with aneuploidy: hygromycin B (ribosome inhibitor), rapamycin (TOR
179 pathway inhibitor), methyl methanesulfonate (MMS, DNA damage inducer) and
180 benomyl (microtubule depolymerizer) (Fig. 2A). Drug concentrations were titrated to
181 reduce wild-type growth by ~80%. Growth was unaffected by the solvent used to
182 resuspend the drugs (Supplemental Fig. S1E). Aneuploidy substantially altered the

183 cellular response to hygromycin, rapamycin, and benomyl, as growth rates no longer
184 scaled with number of genes on aneuploid chromosomes (Fig. 2B). By contrast, MMS
185 treatment showed fewer aneuploidy-associated phenotypes. The percentage of
186 strains displaying substantial relative resistance (normalized growth in the
187 presence/absence of the drug > 2) across the entire library varies greatly between the
188 different drugs ranging from 59% for benomyl to 9% for MMS (Supplemental Fig. S2B,
189 C). We conclude that the capacity for aneuploidy to provide resistance is drug
190 dependent.
191
192 In addition to drug resistance, we also observed frequent drug sensitivity. This was
193 most pronounced for hygromycin, where over 78% of strains showed a greater than
194 two-fold relative decrease in growth in the presence of the drug. Additionally, we
195 measured sensitivity to two stress conditions other than drugs: 39°C for heat stress
196 and 18°C for cold stress. Neither of these conditions greatly influenced cell growth in
197 the euploid strain. However, heat stress led to a two-fold decrease in growth for 66%
198 of the disomic strains, which scaled with the degree of aneuploidy (Supplemental
199 Fig. S2A-C). These results suggest that aneuploid yeast are especially sensitive to
200 hygromycin and heat stress, which implicate translation inhibition and protein
201 misfolding as potential vulnerabilities in aneuploid cells. This would agree with
202 previous reports that aneuploid strains frequently exhibit decreased ribosome levels
203 and proteotoxic stress (Oromendia et al. 2012; Terhorst et al. 2020).
204
205 We next wanted to determine if combinations of aneuploid chromosomes show
206 stronger phenotypes than individual chromosomes. For hygromycin, rapamycin and
207 benomyl, specific chromosome combinations had the highest levels of drug
208 resistance, despite their decreased fitness in the absence of the drugs (Fig. 2C).
209 Notably, absolute resistance to hygromycin was observed only for chromosome
210 combinations, as none of the single disomies grew better than the euploid strain in the
211 presence of hygromycin. To determine if the strength of resistance for chromosome
212 combinations can be predicted based on the single disomies, we compared the growth
213 of double disomies to the product of the single disomies (Supplemental Fig. S2D).
214 Similar to what we observed under standard growth conditions, the predicted and
215 measured growth correlate well for all four drug treatments. This suggests that the
216 majority of the phenotypes for chromosome combinations are additive, and that

217 increased expression of additional resistance genes outweighs the negative effects
218 from the increased expression of all of the other genes when aneuploidies are
219 combined. However, there were some substantial outliers, suggesting that
220 chromosome copy number interactions also play a role in drug resistance/sensitivity
221 (Supplemental Fig. S2D). Overall, we conclude that the strongest drug resistance
222 aneuploidy phenotypes typically come from the combined effects of multiple genes on
223 different chromosomes.
224
225 **Benomyl resistance correlates with α-Tubulin expression in aneuploid strains.**
226 Surprisingly, a majority (59%) of disomic chromosome combinations were resistant to
227 the microtubule depolymerizing factor benomyl (Supplemental Fig. S2B, C). This high
228 percentage results from 6 of the 14 tested single disomic chromosomes conferring
229 substantial resistance to benomyl (Fig. 2C, 3A). Aneuploidy frequently leading to
230 resistance to microtubule inhibitors was not specific to benomyl, as four of the same
231 aneuploid chromosomes provided resistance to another microtubule depolymerizing
232 drug, nocodazole (Supplemental Fig. S3A). We first focused on chromosome 13, as it
233 contains both α-tubulin genes (*TUB1* and *TUB3*). Heterozygous deletion of *TUB3* in
234 the chromosome 13 disomic strain eliminated the resistance phenotype,
235 demonstrating that this gene contributes to the resistance (Supplemental Fig. S3B).
236 To determine if α-tubulin protein abundance contributes to benomyl resistance in the
237 other aneuploid strains, we measured the expression levels in all 14 disomic strains
238 via quantitative western blots. We found that multiple single disomies alter α-tubulin
239 expression levels (Fig. 3B). The measured α-tubulin expression levels correlated well
240 with those measured by high-throughput proteomics of aneuploid yeast strains,
241 demonstrating that these differences occur independently of the measurement method
242 and strain background (Supplemental Fig. S3C, (Muenzner et al. 2024)). Elevated α-
243 tubulin expression levels strongly correlated with the degree of benomyl resistance for
244 the single disomies, suggesting that this is a major mechanism of resistance (Fig. 3C).
245 Intriguingly, only chromosome 12 disomy is extremely sensitive to benomyl and is also
246 the only disomy that shows a substantial decrease in α-tubulin expression. The
247 correlation with benomyl resistance was much weaker for β-tubulin expression (Fig.
248 3C, Supplemental Fig. S3D). These results demonstrate that there are multiple genes
249 across the genome that can alter tubulin expression levels when present at an extra

250 copy, and these mild expression changes can greatly alter the response to microtubule
251 inhibitors.
252
253 **Identification of chromosome arms necessary for aneuploidy-based drug**
254 **resistance.**
255 We next aimed to determine which regions of particular chromosomes provide
256 resistance when gained by a single copy. We focused primarily on benomyl resistance,
257 since six individual disomies led to strong resistance to the drug. This provided
258 multiple examples to systematically examine how many regions/genes typically
259 contribute to positive aneuploidy phenotypes for single aneuploid chromosomes. One
260 possibility is that a single strong resistance gene on each chromosome could be
261 sufficient to give a substantial fitness advantage under harsh drug conditions (single
262 gene model). Another possibility is that multiple mildly beneficial genes on single
263 chromosomes may act together to create strong resistance phenotypes (combinatorial
264 model) (Fig. 4A).
265
266 To determine which regions of chromosomes have negative, positive, or neutral effects
267 on growth with and without benomyl, we implemented a method that deletes part of a
268 chromosome from the end and replaces it with a selection marker and an artificial
269 telomere (Linder et al., 2017) (Fig. 4B). We first generated single arm disomies of all
270 of the benomyl resistant single disomic chromosomes. The deletion of one of the two
271 copies of the chromosome arms was confirmed by qPCR. As with whole chromosome
272 disomies, arm-level disomies have decreased growth rates proportional to the number
273 of aneuploid ORFs under standard conditions (Fig. 4C). Benomyl resistance was
274 frequently associated with a single arm. For chromosomes 2, 4, 10, and 14, disomy of
275 the larger arm was sufficient to fully recapitulate the benomyl resistance, whereas
276 chromosome 13 only showed resistance with disomy of the shorter arm (Fig. 4D). Both
277 α-tubulin genes (*TUB1 and TUB3)* are on the short (left) arm of chromosome 13.
278 Intriguingly, neither of the chromosome 5 arm disomies recapitulated the benomyl
279 resistance of the whole chromosome disomy. Chromosome 5 left arm disomy shows
280 no resistance, while the right arm disomy is only mildly resistant. Therefore, the
281 benomyl resistance for chromosome 5 results from at least one gene on each of the
282 two chromosome arms (Fig. 4D). Overall, the correlation between growth with and
283 without benomyl for the arm-level disomies was not significant, demonstrating that

284 benomyl resistance is not the result of slow growth or a general aneuploidy phenotype
285 (Supplemental Fig. S4A). Instead, resistance likely results from the increased
286 expression of one or more specific genes on the aneuploid chromosome arms.
287
288 Next, we used our arm level aneuploidies to analyze resistance or sensitivity to the
289 three other drugs tested: hygromycin, MMS and rapamycin (Supplemental Fig. S4B).
290 Similar to benomyl, resistance to MMS, rapamycin and hygromycin was primarily
291 associated with single chromosome arms (3/3). By contrast, arm-level aneuploidies
292 generally did not fully recapitulate increased drug sensitivity phenotypes (Fig. 4E,
293 Supplemental Fig. S4B, C). Instead, both arms often showed partial sensitivity. This is
294 also the case for the only chromosome that showed strong sensitivity to benomyl,
295 chromosome 12 (Fig. 4D). These results suggest that aneuploidy-based drug
296 sensitivity results from the combined effects of more genes than drug resistance.
297 Surprisingly, in some examples, drug sensitivity from one chromosome arm was
298 compensated for by the resistance from the second chromosome arm (2/8)
299 (Supplemental Fig. S4B, C).

300 **Most aneuploidy-based drug resistance phenotypes come from the combined**
301 **effect of multiple genes**

302 Since most of the resistance phenotypes were associated with the larger arms, we
303 wanted to determine how many regions/genes on these arms contribute to benomyl
304 resistance. We therefore made multiple shorter deletions to the benomyl resistant
305 disomies to identify regions of drug resistance. For example, seven additional cuts
306 were made on the right arm of chromosome 4 to identify regions of interest. As the
307 size of the chromosome decreased, growth under standard conditions gradually
308 increased (Fig. 5A). This further demonstrates that the negative effects on fitness for
309 aneuploid strains result from many genes across the length of a chromosome (Bonney
310 et al. 2015). Conversely, benomyl resistance decreased in a stepwise manner
311 following the deletion of three independent regions on the right arm (Fig. 5A). For 5 of
312 the 6 resistant chromosomes, we identified at least two regions that contributed to
313 resistance, with the most being 5 regions for chromosome 5 (Fig. 5C,
314 Supplemental Fig. S5). Interestingly, three of the benomyl resistant chromosomes
315 also had regions that increased drug sensitivity (Fig. 5A, C, Supplemental Fig. S5A).

316 The strength of drug resistance is therefore a balance between regions that confer
317 resistance and sensitivity.
318
319 We next aimed to identify the resistance genes within the identified regions. The
320 regions each contain between ~30 and 100 genes. We identified candidate genes by
321 looking for: sensitivity to benomyl in high-throughput screens of the yeast knockout
322 collection, essential genes, and genes that have GO Terms associated with
323 tubulin/microtubules. Candidate genes were tested via heterozygous deletions in the
324 disomic strains (Supplemental Fig. S6A). For the two regions on chromosome 4
325 associated with the strongest benomyl resistance, we identified single gene deletions
326 that decreased resistance to a similar extent as deleting the entire chromosomal
327 region (Fig. 5B, C). In total, we identified 9 genes that decrease the resistance of
328 aneuploid chromosomes when deleted heterozygously (Supplemental Fig. S6A, S7).
329 In addition to *TUB3* on chromosome 13, we identified two additional genes associated
330 with tubulin expression (*GIM4*-chr.5, *PFD1*-chr.10). Both of these genes are members
331 of the prefoldin complex, which is a chaperone that promotes the proper folding of α-
332 and β-tubulin. One resistance gene is involved in microtubule stabilization (*BIM1*-
333 chr.5). Interestingly, two of the resistance genes have recently been implicated in the
334 spindle position checkpoint (*SWR1*-chr.4, *MCK1*-chr.14) (Rathi et al. 2022; Caydasi et
335 al. 2023). Another resistance gene, *TOF1*-chr.14, is primarily associated with
336 protection of the DNA replication fork. However, it shows a synthetic lethal interaction
337 with *BIM1*, indicating an additional role in chromosome segregation (Tong et al. 2004;
338 Pan et al. 2004). Overall, we have identified many genes across the genome that
339 contribute to aneuploidy-based benomyl resistance.
340
341 In addition to the disomic chromosomes that lead to benomyl resistance, we also
342 identified chromosomal regions that lead to rapamycin resistance on chromosome 10.
343 Strains with disomy of chromosome 10 have previously been shown to be rapamycin
344 resistant (Torres et al. 2007). This was speculated to be due to the presence of the
345 *TOR1* gene. Heterozygous deletion of *TOR1* in a chromosome 10 disomic strain only
346 partially decreased rapamycin resistance, indicating that there are more genes on
347 chromosome 10 that contribute to the phenotype (Supplemental Fig. S6B).
348 Furthermore, both chromosome arms contribute to rapamycin resistance

349 (Supplemental Fig. S6C). We conclude that the combined overexpression of multiple
350 genes leading to strong phenotypes is a common feature of aneuploidy.

351 **The strongest aneuploidy phenotypes result from synergistic effects**

352 Chromosome 5 disomy has the strongest benomyl resistance phenotype and is the
353 only chromosome where both arms contribute to the phenotype (Fig. 4D). Additionally,
354 the degree of resistance for the whole chromosome was substantially higher than
355 either of the two individual arm-level disomies, suggesting a synergistic interaction
356 between the two arms. To look at this more systematically, we predicted the strength
357 of resistance for whole chromosome aneuploidy based on the resistance of the
358 individual arm-level aneuploidies (Fig. 6A). Although the other single disomies
359 displayed resistance in line with the predictions, benomyl resistance for chromosome
360 5 was substantially higher than predicted. This demonstrates a strong synergistic
361 interaction between the two arms.
362
363 We next wanted to determine if the strongest phenotypes for double disomic strains
364 also result from synergistic interactions. We focused on chromosome combinations
365 where the single disomies on their own were benomyl resistant. We initially observed
366 that the combined disomies of chromosomes 2 & 4 and 2 & 13 are exceptionally
367 strong, showing robust resistance even at higher benomyl concentrations (Fig. 6B).
368 These combinations are as resistant as a deletion mutation known to be highly
369 resistant to benomyl (Schibler et al. 2016), despite strong growth defects for aneuploid
370 strains in the absence of the drug (Fig. 6C). Looking at combinations with chromosome
371 2 specifically, we observed a wide range of resistance phenotypes, ranging from
372 strong positive to strong negative interactions (Fig. 6B, Supplemental Fig. S8A).
373 Strikingly, a strong negative genetic interaction between chromosomes 2 and 14
374 results in the near-complete loss of the benomyl resistance (Fig. 6B, D). Almost all
375 combinations with chromosome 14 grow worse than the single disomies
376 (Supplemental Fig. S8B), indicating a general negative effect of chromosome 14
377 combinations and benomyl resistance. We also observed a positive synergistic
378 interaction between chromosomes 3 and 12 for rapamycin resistance, demonstrating
379 that such interactions are not benomyl-specific (Supplemental Fig. S8C). We conclude
380 that although most aneuploidies display additive effects between genes, regions, and

chromosomes, the strongest beneficial growth phenotypes often come from synergistic interactions.

Discussion

In this study, we generated a library of engineered single and double aneuploid yeast strains to systematically determine the genetic drivers of aneuploidy-based drug resistance. In addition, we used a comprehensive approach to identify regions/genes on aneuploid chromosomes that contribute to aneuploidy phenotypes. This approach has numerous advantages, allowing for the identification of: i) multiple regions on a chromosome that contribute to a phenotype, ii) both resistant and sensitive regions on a single chromosome, iii) regions that act synergistically, where each region on its own would not have a strong phenotype. Together, these strategies provide a means to comprehensively identify the genetic determinants of positive and negative selection for aneuploid chromosomes either alone or in combination.

When measuring the resistance of the chromosome gain collection to different inhibitors, the strongest resistance phenotypes were consistently identified for chromosome combinations. This demonstrates that altered copy numbers of multiple genes combine to create stronger beneficial aneuploidy phenotypes. These additional benefits are observed despite the often substantial negative growth phenotypes for the double aneuploid strains under optimal growth conditions. Therefore, the benefits of combining multiple aneuploid chromosomes generally outweigh the downsides under selective conditions. This combinatorial behavior of aneuploid chromosomes could explain the frequent occurrence of complex aneuploidy in both adapted yeast populations and cancer karyotypes (Mitelman Database of Chromosome Aberrations and Gene Fusions in Cancer, 2025. https://mitelmandatabase.isb-cgc.org, Rancati et al. 2008; Ravichandran et al. 2018; Peter et al. 2018; Klockner and Campbell 2024).

In addition to identifying strong phenotypes for combinations of aneuploid chromosomes, we discovered multiple regions within individual chromosomes that contribute to drug resistance phenotypes. We identified up to 5 regions on a single chromosome that contribute to drug resistance, emphasizing that multiple genes are typically responsible for strong aneuploidy phenotypes. This combinatorial action of

415 many genes suggests an advantage for the selection of aneuploidy over other types
416 of genomic alterations. Changing the expression of genes with distinct and
417 complementary functions may provide proliferative benefits that could not be
418 accomplished through single mutations. These data provide substantial support for a
419 "combinatorial genes" explanation for the specific benefits of aneuploidy over other
420 genomic alterations.
421
422 Increasing the degree of selection via higher concentrations of benomyl revealed
423 strong positive synergistic interactions between aneuploid chromosomes. We also
424 observed a clear synergistic interaction between the arms of chromosome 5. These
425 results suggest another possible advantage for adaptation through aneuploidy,
426 wherein the altered expression levels of two complementary genes would not be
427 selected for individually due to a lack of phenotype. However, two simultaneous
428 changes to the genome through a single chromosome missegregation event would
429 enable their combined selection, leading to a strong beneficial phenotype. These
430 results, along with the recently discovered synergistic interaction between
431 chromosomes 3 and 6 in multi-azole tolerance of the human pathogen *Candida*
432 *albicans* (Zhou et al. 2024), demonstrate that positive synergistic interactions are more
433 heavily selected for under higher stress conditions. We also find that combining
434 beneficial aneuploidies can occasionally lead to weaker than expected phenotypes,
435 highlighting that negative genetic interactions also likely impact complex karyotype
436 formation. Positive and negative genetic interactions between co-occurring
437 aneuploidies have been suggested based on correlations between chromosome arm
438 frequencies in cancer aneuploidy patterns (Ravichandran et al. 2018). Such co-
439 occurrence patterns can be highly predictive of disease progression and
440 chemotherapy resistance in cancer (Shukla et al. 2020).
441
442 The main drivers of beneficial aneuploidy phenotypes are alterations in expression
443 levels resulting from gene copy number changes of specific resistance-driving genes
444 (Selmecki et al. 2009; Chen et al. 2012; Ravichandran et al. 2018; Barney et al. 2021;
445 Ryu et al. 2016; Zhou et al. 2024; Pavani et al. 2021; Beaupere et al. 2018; Linder et
446 al. 2017; Adell et al. 2023; Watson et al. 2024). We observed a significant correlation
447 between growth on benomyl and altered α-tubulin expression levels. In addition to

TUB3 on chromosome 13, two members of the prefoldin complex (*GIM4*-chr. 5, *PFD1*-chr. 10) contribute to aneuploidy-based benomyl resistance. Intriguingly, chromosome 12 disomy decreases tubulin expression levels and is very sensitive to microtubule destabilization via benomyl. This decrease in tubulin levels for chromosome 12 disomy could also help explain how it rescues microtubule hyperstabilization (Macaluso et al. 2025). We conclude that tubulin expression levels are not tightly regulated in yeast. Furthermore, even relatively small changes in α-tubulin expression levels can substantially influence resistance and sensitivity to microtubule inhibitors. These findings underscore the importance of recognizing subtle (<2-fold) expression changes, as they have the capacity for causing strong phenotypes.

Not all of the genes that contributed to benomyl resistance have functions related to tubulin expression. We identified two components of the spindle position checkpoint (*MCK1*-chr. 14, *SWR1*-chr. 4), implicating this checkpoint in mitigating the effects of microtubule-targeting drugs. We also identified a drug exporter (*SNQ2*-chr. 4) and a microtubule stabilizer (*BIM1*-chr. 5). Importantly, the genes that we identified for resistant chromosome region were not always the most obvious candidates (Supplemental Fig. S7). *TOF1*-chr. 14 and *SAP1*-chr. 5 have not previously been associated with microtubule functions, but both contribute to benomyl resistance on their respective aneuploid chromosomes. These results highlight the need for unbiased approaches to determine the genes responsible for aneuploidy phenotypes, as phenotypes resulting from mild changes in expression could greatly differ from those that come from inhibition/deletion.

While mild overexpression of specific genes can confer drug resistance, the overexpression of many genes across an entire chromosome greatly increases aneuploidy-induced cellular stress (Torres et al. 2007; Sheltzer et al. 2011; Oromendia et al. 2012; Thorburn et al. 2013; Beach et al. 2017; reviewed in Li and Zhu 2022). This stress presents potential targets to selectively eliminate aneuploid cells (Cohen-Sharir et al. 2021; Ippolito et al. 2024). However, the potential to leverage aneuploidy-based sensitivities requires a deeper understanding of the underlying mechanisms driving these vulnerabilities. 78% of the strains in the chromosome gain collection were sensitive to hygromycin B and 66% were sensitive to heat stress (Supplemental Fig. S2C). These results provide additional support for decreased ribosome function and

482 proteotoxic stress as hallmarks of aneuploidy (Oromendia et al. 2012; Terhorst et al.
483 2020). By contrast, inducing DNA damage via MMS did not result in large scale
484 sensitivity, suggesting aneuploidy-induced genome instability may be more
485 chromosome specific. Despite the general sensitivity to hygromycin, we identified a
486 few strong examples of aneuploidy-driven hygromycin resistance. Additionally,
487 sensitivity of one chromosome arm can be masked by resistance of the other arm
488 (Supplemental Fig. S4B, C). Together, these results demonstrate that regions of the
489 genome that contribute to sensitivity or resistance can fully or partially counteract each
490 other. Sensitivity and negative selection have been predicted to be strong drivers of
491 cancer karyotype evolution, potentially even more so than positive selection (Jubran
492 et al. 2024).
493
494 Given the high prevalence of aneuploidy in cancer, it is an attractive target for
495 identifying exploitable vulnerabilities. Initially, focus has been placed on vulnerabilities
496 resulting from aneuploidy in general, as opposed to ones created by specific
497 chromosomes. Currently, one of the leading candidates for targeting a general
498 vulnerability of aneuploidy is proteotoxic stress, as it has been found in both yeast and
499 human cells with a wide variety of aneuploid karyotypes (Tang et al. 2011; Oromendia
500 et al. 2012; Stingele et al. 2012). Our results showing a general sensitivity to heat
501 stress across dozens of engineered aneuploid strains would agree with proteotoxic
502 stress as a good candidate and may additionally suggest that localized hyperthermia
503 therapy (reviewed in Hannon et al. 2021) may be especially effective on highly
504 aneuploid tumors. We also observed a general sensitivity to the ribosome inhibitor
505 hygromycin B for the majority of aneuploid strains, implicating protein synthesis as an
506 additional candidate for targeting aneuploid cells. However, specific chromosome
507 disomies were not sensitive to the drug and could even provide resistance. These
508 chromosome-specific differences suggest that even for effective general aneuploidy-
509 targeting treatments, certain karyotypes may not respond well and that linking cancer
510 karyotypes to drug responses could greatly improve treatment effectiveness and
511 choice. Additional efforts have recently been made to identify vulnerabilities of specific
512 aneuploid chromosomes (Cai et al. 2016; Huth et al. 2023; Girish et al. 2023). Our
513 work also supports this strategy, as we identified frequent chromosome-specific drug
514 sensitivities.

515 **Material and methods**

516 *Yeast strains and media*

517 All yeast strains and plasmids used in this study are listed in Supplemental Table S2, S3.
518 All yeast strains are derivatives of BY4741 and BY4742. All yeast strains were cultured in
519 complete synthetic media (CMS) lacking histidine, uracil, lysine, and leucine and
520 cultured at 30 °C, unless otherwise stated. For 5-FOA (Chempur, Karlsruhe, Germany,
521 220141- 70-8) selection, a concentration of 1 mg/mL was used. Growth assays were
522 always conducted in yeast extract/peptone containing 40 µg/ml adenine-HCl (YPA) and
523 2% glucose (YPAD) in liquid cultures and plate-based assays. For high-throughput drug
524 resistance screens, 17.5 µg/ml benomyl (Sigma-Aldrich), 40 µg/ml hygromycin B (Carl
525 Roth), 0.02 % MMS (Sigma-Aldrich) or 5 nM rapamycin (Santa Cruz Biotechnology) were
526 added to YPAD agar plates. YPAD + DMSO agar plates were used as controls for drugs
527 dissolved in DMSO. Genetic manipulations such as insertions and gene deletions were
528 conducted as previously described (Longtine et al. 1998). Strains inducible for
529 aneuploidy were generated using a conditional centromere, as described in Anders et al.
530 (2009). Single disomies and double disomies were engineered as described in
531 (Ravichandran et al. 2018). Each disomy was generated independently with two different
532 pairs of auxotrophic markers (*URA3* and *HIS3*; *LYS2* and *LEU2*). For engineering
533 monosomies, one copy of the endogenous centromere was replaced by P_{GAL1}-*CEN3*
534 *URA3*. Flow cytometry of selected strains was used to detect potential changes in ploidy
535 and exclude strains that spontaneously diploidized.

536

537 *PCR-mediated partial chromosome deletions*

538 PCR-mediated partial chromosome deletions were implemented as described in Linder
539 et al. (2017). To generate a deletion, a 500-800 bp fragment homologous to the intended
540 cut-site was combined with a resistance marker (*kanMX* or *hphNT1*) and a telomeric seed
541 sequence. The telomeric seed sequence (6x 5'CCCCAA3') was added at the 3' end of the
542 primer binding the resistance cassette. The homology sequence was PCR amplified from
543 genomic DNA with an added 30 bp homology sequence to the resistance cassette.
544 Fragments were combined using overlap extension PCR.

545 *High-throughput growth measurements*

546 For monosomies, chromosome missegregation was induced immediately before plating.
547 Strains were grown for 18h in 2 ml deep-well plates in 200 µl YPAD at 30 °C (shaking). 4 µl
548 were transferred to 150 µl of YPA plus 1% raffinose (YPAR) and grown to log phase (~4h).
549 50 µl of YPA medium containing 4% galactose were added and grown for 3h to induce
550 chromosome missegregation. Samples were plated on 5-FOA agar plates using a ROTOR
551 HDA robot for high-throughput plating (Singer Instruments, Roadwater, UK). Images were
552 taken after 24, 48 and 72h. The chromosome gain collection was grown in 2 ml deep-well
553 plates in 200 µl CSM lacking histidine, uracil, leucine and lysine at 30 °C. After 18h,
554 cultures were diluted 1:10 in 1 × PBS and plated with the ROTOR HDA onto condition
555 specific YPAD plates. Strains were grown at 30 °C (if not indicated otherwise) and images
556 were taken at different time points from 24 to 72 h.
557

558 *Doubling time measurements*

559 Overnight cultures were grown in CSM lacking histidine, uracil, leucine and lysine,
560 diluted in YPAD and grown for 4h to mid log-phase. Cultures were diluted to an optical
561 density at 600 nm of 0.02 in 200 µl YPAD in 96-well plates. OD measurements were
562 taken every 15 min for 24 h using a Synergy S1 plate reader (BioTek Instruments, Inc.,
563 Luzern, Switzerland).

564

565 *Serial dilutions*

566 Strains were grown over night in CSM lacking histidine, uracil, leucine and lysine.
567 Cultures were diluted in fresh media (OD ~ 0.05) and grown to log phase (OD ~0.45),
568 normalized by OD, diluted in 1 x PBS (1 : 10) and plated on condition specific agar
569 plates.
570

571 *High-throughput growth assay quantification and analysis*

572 Images of yeast colonies on plates were quantified using ImageJ (National Institute of
573 Health). Integrated densities of each spot area and surrounding area were quantified.
574 Background subtraction was done for each spot area individually by subtracting the

surrounding intensity from the colony intensity (Supplemental data file). For comparing growth of chromosome loss strains to chromosome gain strains, 10 representative chromosome loss strains were spotted on YPAD after selection on 5-FOA plates and measured for colony intensity. These values were then used to adjust the growth measurements for the other chromosome loss strains. Growth rate prediction of double disomies and double monosomies in high throughput experiments was predicted by multiplying the growth of the two individual single disomies/monosomies. This was done for each treatment individually. Determination of genetic interactions between disomic chromosomes were calculated from dilution series by adding the measurements of the individual single disomies (DisA + DisB - 1). Growth rates greater/smaller than additive prediction +/- 30% were classified as synergistic genetic interaction. The same method was used to identify genetic interactions between chromosome arms.

qPCR

For DNA extraction, cells were taken from plates and lysed in 20 µl of 0.02 M NaOH for 10 min at 100 °C. Lysates were centrifuged for 10 min on a mini-centrifuge (Thermo Fisher Scientific) to pellet cellular debris. Each 20 µl reaction contained 10 µl of Luna qPCR Mastermix (New England BioLabs Inc.), 1 µl of lysate and 140 nM of each primer. Measurements were made on a RealPlex2 qPCR machine (Eppendorf). Cycling conditions were: activation/denaturation for 5 min at 95 °C followed by 40 cycles of 15 sec at 95 °C, 1 min at 60 °C with a subsequent fluorescence measurement. Melting curves were generated to determine primer specificity. *Ct* values were determined using the automatic thresholding of the RealPlex2 software. Chromosome copy numbers were calculated using a slightly modified ΔΔCt method (Schmittgen 2001). The Ct values from duplicates were averaged and used to obtain the ΔCt, which was raised to the negative power of 2 to give the fold change. The ratio of fold change of the test strains to that of a wild-type strain was calculated to obtain the chromosome copy numbers. Karyotyping primers are in Supplemental Table S5.

604 *Protein extraction and Western blotting*

605 For protein extraction, saturated ON cultures were diluted to an OD of 0.02 into YPAD.
606 Cells were grown to an OD of ~0.6, normalized by OD and harvested. Proteins were
607 extracted by pelleting cells, resuspending them in 100 µl ddH_2O, adding 100 µl 0.2 M
608 NaOH and incubating them at room temperature for 5 min. Cells were pelleted and
609 resuspended in 1x sample buffer before incubating them at 95° C for 3 min. Samples
610 were stored at -20°C. Membranes were stained with 0.1 % Ponceau S (Sigma Aldrich) in
611 5% acetic acid. Total protein amount was detected with the ChemiDocMP imaging
612 system (Bio-Rad). Membranes were washed for 30 min in Tris-buffered saline with 0.01%
613 Tween (TBS-T) with three buffer exchanges, blocked for 1 h in 5% BSA (Sigma-Aldrich) or
614 5% skim milk (Gerbu Biotechnik GmbH) in TBS-T, depending on the primary antibody (see
615 below). Primary antibodies diluted in their respective blocking buffers were incubated
616 overnight at 4°C on an orbital shaker. Membranes were washed for 30 min in TBS-T with
617 three buffer exchanges before and after secondary antibody incubation. Horseradish
618 peroxidase (HRP)-conjugated antimouse IgG secondary antibody (1:10,000; Cell
619 Signaling Technology 7076) diluted in the respective blocking buffers was incubated for 1
620 h at room temperature. Chemiluminescence was developed using the Amersham ECL
621 Prime detection reagent (Cytiva) and detected with the ChemiDocMP. Protein bands were
622 quantified using ImageJ and normalized to the total protein amount quantified from the
623 Ponceau S staining. The following primary antibodies were used: mouse anti-Pgk1 (in BSA
624 and skim milk–TBST, respectively; 1:20.000; Thermo Fisher Scientific 22C5D8), anti-α-
625 Tubulin (in skim milk–TBS; 1:20,000; mouse; Sigma-Aldrich T6074), anti-β-Tubulin (in
626 BSA; 1:5.000; mouse; Developmental Studies Hybridoma Bank E7).
627

628 *Flow Cytometry*

629 Cultures were grown to log-phase, pelleted and resuspended in 300 µl H_2O. 700 µl of
630 100 % EtOH were added during vertexing, and cells were fixed for 1h at room
631 temperature. Cells were pelleted and resuspended in 50 mM sodium citrate, sonicated
632 to disperse cell clumps and treated with 250 µg/mL RNase A (Sigma-Aldrich, R6513) and
633 1 mg/mL Proteinase K (Sigma-Aldrich, P2308) overnight at 37°C. Cells were resuspended
634 in 50 mM sodium citrate solution containing 1 µM SYTOX green (Thermo Fisher,

635 10768273). Samples were run on BD LSRFortessa Cell Analyzer equipped with a 15-mW
636 488-nm laser. Maximum count peaks for fluorescence intensities were calculated using
637 the BD FACSDiva 8.0.1 software.
638

639 *Statistical analysis*

640 Statistical analysis was performed using GraphPad Prism software. Details for the
641 statistical tests used in a particular experiment are reported in the figure legends.
642
643
644

Competing interest statement

The authors declare no competing interests.

Acknowledgements

The authors thank the Campbell and Dammermann laboratories for helpful discussions and comments. We thank the Kraft lab and Kirk Anders for gifts of strains and plasmids and Alexander Dammermann and Sean Montgomery for careful reading of the manuscript. We acknowledge the service of the FACS Facility.

This work was supported by a Max Perutz Labs Fellowship to M.S.K and the Austrian Science Fund (FWF) grant F 8802-B to C.S.C.

Author Contributions

M.S.K conducted the majority of the experiments. M.S.K., S.F., M.C.R and C.H., generated the chromosome gain collection. C.H. and S.F. generated the chromosome loss collection. C.H. performed growth measurements and analysis of the chromosome loss collection. M.S.K. and C.S.C conceptualized the research, analyzed the data, and wrote the manuscript. All authors reviewed and approved the manuscript.

References

Adell MAY, Klockner TC, Höfler R, Wallner L, Schmid J, Markovic A, Martyniak A, Campbell CS. 2023. Adaptation to spindle assembly checkpoint inhibition through the selection of specific aneuploidies. *Genes Dev* **37**: 171–190.

Anders KR, Kudrna JR, Keller KE, Kinghorn BAA, Miller EM, Pauw D, Peck AT, Shellooe CE, Strong IJT. 2009. A strategy for constructing aneuploid yeast strains by transient nondisjunction of a target chromosome. *BMC Genet* **10**: 1–11.

Barney JB, Chandrashekarappa DG, Soncini SR, Schmidt MC. 2021. Drug resistance in diploid yeast is acquired through dominant alleles, haploinsufficiency, gene duplication and aneuploidy. *PLOS Genet* **17**: e1009800.

Beach RR, Ricci-Tam C, Brennan CM, Moomau CA, Hsu P, Hua B, Silberman RE, Springer M, Amon A. 2017. Aneuploidy Causes Non-genetic Individuality. *Cell* **169**: 229-242.e21.

Beaupere C, Dinatto L, Wasko BM, Chen RB, VanValkenburg L, Kiflezghi MG, Lee MB, Promislow DEL, Dang W, Kaeberlein M, et al. 2018. Genetic screen identifies adaptive aneuploidy as a key mediator of ER stress resistance in yeast. *Proc Natl Acad Sci* **115**: 9586–9591.

Bonney ME, Moriya H, Amon A. 2015. Aneuploid proliferation defects in yeast are not driven by copy number changes of a few dosage-sensitive genes. *Genes Dev* **29**: 898–903.

Cai Y, Crowther J, Pastor T, Abbasi Asbagh L, Baietti MF, De Troyer M, Vazquez I, Talebi A, Renzi F, Dehairs J, et al. 2016. Loss of Chromosome 8p Governs Tumor Progression and Drug Response by Altering Lipid Metabolism. *Cancer Cell* **29**: 751–766.

Caydasi AK, Khmelinskii A, Darieva Z, Kurtulmus B, Knop M, Pereira G. 2023. SWR1 chromatin remodeling complex prevents mitotic slippage during spindle position checkpoint arrest. *Mol Biol Cell* **34**: ar11.

Chen G, Bradford WD, Seidel CW, Li R. 2012. Hsp90 stress potentiates rapid cellular adaptation through induction of aneuploidy. *Nature* **482**: 246–250.

Clarke MN, Marsoner T, Adell MAY, Ravichandran MC, Campbell CS. 2023. Adaptation to high rates of chromosomal instability and aneuploidy through multiple pathways in budding yeast. *EMBO J* **42**: e111500.

Cohen-Sharir Y, McFarland JM, Abdusamad M, Marquis C, Bernhard SV, Kazachkova M, Tang H, Ippolito MR, Laue K, Zerbib J, et al. 2021. Aneuploidy renders cancer cells vulnerable to mitotic checkpoint inhibition. *Nature* **590**: 486–491.

Girish V, Lakhani AA, Thompson SL, Scaduto CM, Brown LM, Hagenson RA, Sausville EL, Mendelson BE, Kandikuppa PK, Lukow DA, et al. 2023. Oncogene-like addiction to aneuploidy in human cancers. *Science* **381**: eadg4521.

704 Gresham D, Desai MM, Tucker CM, Jenq HT, Pai DA, Ward A, DeSevo CG, Botstein D,
705 Dunham MJ. 2008. The Repertoire and Dynamics of Evolutionary Adaptations to
706 Controlled Nutrient-Limited Environments in Yeast. *PLoS Genet* **4**: e1000303.

707 Hannon G, Tansi FL, Hilger I, Prina-Mello A. 2021. The Effects of Localized Heat on the
708 Hallmarks of Cancer. *Adv Ther* **4**: 2000267.

709 Hose J, Escalante LE, Clowers KJ, Dutcher HA, Robinson D, Bouriakov V, Coon JJ,
710 Shishkova E, Gasch AP. 2020. The genetic basis of aneuploidy tolerance in wild
711 yeast. *eLife* **9**.

712 Huth T, Dreher EC, Lemke S, Fritzsche S, Sugiyanto RN, Castven D, Ibberson D, Sticht C,
713 Eiteneuer E, Jauch A, et al. 2023. Chromosome 8p engineering reveals increased
714 metastatic potential targetable by patient-specific synthetic lethality in liver
715 cancer. *Sci Adv* **9**: eadh1442.

716 Ippolito MR, Martis V, Martin S, Tijhuis AE, Hong C, Wardenaar R, Dumont M, Zerbib J,
717 Spierings DCJ, Fachinetti D, et al. 2021. Gene copy-number changes and
718 chromosomal instability induced by aneuploidy confer resistance to
719 chemotherapy. *Dev Cell* **56**: 2440-2454.e6.

720 Ippolito MR, Zerbib J, Eliezer Y, Reuveni E, Viganò S, Taglietti S, Scorzoni S, Gianotti S,
721 Martin S, Muenzner J, et al. 2024. Increased RNA and protein degradation is
722 required for counteracting transcriptional burden and proteotoxic stress in
723 human aneuploid cells. *Cancer Discov* **14**.

724 Jubran J, Slutsky R, Rozenblum N, Rokach L, Ben-David U, Yeger-Lotem E. 2024.
725 Machine-learning analysis reveals an important role for negative selection in
726 shaping cancer aneuploidy landscapes. *Genome Biol* **25**: 95.

727 Kaboli S, Miyamoto T, Sunada K, Sasano Y, Sugiyama M, Harashima S. 2016. Improved
728 stress resistance and ethanol production by segmental haploidization of the
729 diploid genome in Saccharomyces cerevisiae. *J Biosci Bioeng* **121**: 638–644.

730 Klockner TC, Campbell CS. 2024. Selection forces underlying aneuploidy patterns in
731 cancer. *Mol Cell Oncol* **11**: 2369388.

732 Li R, Zhu J. 2022. Effects of aneuploidy on cell behaviour and function. *Nat Rev Mol Cell*
733 *Biol* **23**: 250–265.

734 Linder RA, Greco JP, Seidl F, Matsui T, Ehrenreich IM. 2017. The Stress-Inducible
735 Peroxidase *TSA2* Underlies a Conditionally Beneficial Chromosomal Duplication
736 in *Saccharomyces cerevisiae*. *G3 GenesGenomesGenetics* **7**: 3177–3184.

737 Liu X, Wang X, Yang X, Liu S, Jiang L, Qu Y, Hu L, Ouyang Q, Tang C. 2015. Reliable cell
738 cycle commitment in budding yeast is ensured by signal integration. *eLife* **4**:
739 e03977.

Loegler V, Friedrich A, Schacherer J. 2024. Overview of the *Saccharomyces cerevisiae* population structure through the lens of 3,034 genomes. *G3 Genes Genomes Genet* jkae245.

Longtine MS, McKenzie A, Demarini DJ, Shah NG, Wach A, Brachat A, Philippsen P, Pringle JR. 1998. Additional modules for versatile and economical PCR-based gene deletion and modification in Saccharomyces cerevisiae. *Yeast Chichester Engl* **14**: 953–61.

Lukow DA, Sausville EL, Suri P, Chunduri NK, Wieland A, Leu J, Smith JC, Girish V, Kumar AA, Kendall J, et al. 2021. Chromosomal instability accelerates the evolution of resistance to anti-cancer therapies. *Dev Cell* **56**: 2427-2439.e4.

Macaluso F, Bos T, Chiroli E, Bonaiuti P, Apuan JC, Gross F, Pompei S, Rice LM, Ciliberto A. 2025. Evolutionary adaptation to hyperstable microtubules selectively targets tubulins and is empowered by the spindle assembly checkpoint. *Cell Rep* **44**: 115323.

Mitelman Database of Chromosome Aberrations and Gene Fusions in Cancer (2025). Mitelman F, Johansson B and Mertens F (Eds.), https://mitelmandatabase.isb-cgc.org

Morard M, Macías LG, Adam AC, Lairón-Peris M, Pérez-Torrado R, Toft C, Barrio E. 2019. Aneuploidy and Ethanol Tolerance in Saccharomyces cerevisiae. *Front Genet* **10**: 82.

Muenzner J, Trébulle P, Agostini F, Zauber H, Messner CB, Steger M, Kilian C, Lau K, Barthel N, Lehmann A, et al. 2024. Natural proteome diversity links aneuploidy tolerance to protein turnover. *Nature* **630**: 149–157.

Oromendia AB, Dodgson SE, Amon A. 2012. Aneuploidy causes proteotoxic stress in yeast. *Genes Dev* **26**: 2696–2708.

Pan X, Yuan DS, Xiang D, Wang X, Sookhai-Mahadeo S, Bader JS, Hieter P, Spencer F, Boeke JD. 2004. A Robust Toolkit for Functional Profiling of the Yeast Genome. *Mol Cell* **16**: 487–496.

Pavani M, Bonaiuti P, Chiroli E, Gross F, Natali F, Macaluso F, Póti Á, Pasqualato S, Farkas Z, Pompei S, et al. 2021. Epistasis, aneuploidy, and functional mutations underlie evolution of resistance to induced microtubule depolymerization. *EMBO J* **40**: e108225.

Pavelka N, Rancati G, Zhu J, Bradford WD, Saraf A, Florens L, Sanderson BW, Hattem GL, Li R. 2010. Aneuploidy confers quantitative proteome changes and phenotypic variation in budding yeast. *Nature* **468**: 321–325.

Peter J, De Chiara M, Friedrich A, Yue J-X, Pflieger D, Bergström A, Sigwalt A, Barre B, Freel K, Llored A, et al. 2018. Genome evolution across 1,011 Saccharomyces cerevisiae isolates. *Nature* **556**: 339–344.

Rancati G, Pavelka N, Fleharty B, Noll A, Trimble R, Walton K, Perera A, Staehling-Hampton K, Seidel CW, Li R. 2008. Aneuploidy Underlies Rapid Adaptive Evolution of Yeast Cells Deprived of a Conserved Cytokinesis Motor. *Cell* **135**: 879–893.

Rathi S, Polat I, Pereira G. 2022. The budding yeast GSK-3 homologue Mck1 is an essential component of the spindle position checkpoint. *Open Biol* **12**: 220203.

Ravichandran MC, Fink S, Clarke MN, Hofer FC, Campbell CS. 2018. Genetic interactions between specific chromosome copy number alterations dictate complex aneuploidy patterns. *Genes Dev* **32**: 1485–1498.

Rojas J, Hose J, Dutcher HA, Place M, Wolters JF, Hittinger CT, Gasch AP. 2024. Comparative modeling reveals the molecular determinants of aneuploidy fitness cost in a wild yeast model. *Cell Genomics* **4**: 100656.

Ryu H-Y, Wilson NR, Mehta S, Hwang SS, Hochstrasser M. 2016. Loss of the SUMO protease Ulp2 triggers a specific multichromosome aneuploidy. *Genes Dev* **30**: 1881–1894.

Schibler A, Koutelou E, Tomida J, Wilson-Pham M, Wang L, Lu Y, Cabrera AP, Chosed RJ, Li W, Li B, et al. 2016. Histone H3K4 methylation regulates deactivation of the spindle assembly checkpoint through direct binding of Mad2. *Genes Dev* **30**: 1187–1197.

Schmittgen TD. 2001. Real-Time Quantitative PCR. *Methods* **25**: 383–385.

Selmecki A, Forche A, Berman J. 2006. Aneuploidy and Isochromosome Formation in Drug-Resistant *Candida albicans*. *Science* **313**: 367–370.

Selmecki AM, Dulmage K, Cowen LE, Anderson JB, Berman J. 2009. Acquisition of Aneuploidy Provides Increased Fitness during the Evolution of Antifungal Drug Resistance. *PLoS Genet* **5**: e1000705.

Sheltzer JM, Blank HM, Pfau SJ, Tange Y, George BM, Humpton TJ, Brito IL, Hiraoka Y, Niwa O, Amon A. 2011. Aneuploidy Drives Genomic Instability in Yeast. *Science* **333**: 1026–1030.

Shukla A, Nguyen THM, Moka SB, Ellis JJ, Grady JP, Oey H, Cristino AS, Khanna KK, Kroese DP, Krause L, et al. 2020. Chromosome arm aneuploidies shape tumour evolution and drug response. *Nat Commun* **11**: 449.

Stingele S, Stoehr G, Peplowska K, Cox J, Mann M, Storchova Z. 2012. Global analysis of genome, transcriptome and proteome reveals the response to aneuploidy in human cells. *Mol Syst Biol* **8**: 608.

Su XA, Ma D, Parsons JV, Replogle JM, Amatruda JF, Whittaker CA, Stegmaier K, Amon A. 2021. *RAD21* is a driver of chromosome 8 gain in Ewing sarcoma to mitigate replication stress. *Genes Dev* **35**: 556–572.

Tang Y-C, Williams BR, Siegel JJ, Amon A. 2011. Identification of Aneuploidy-Selective Antiproliferation Compounds. *Cell* **144**: 499–512.

Terhorst A, Sandikci A, Keller A, Whittaker CA, Dunham MJ, Amon A. 2020. The environmental stress response causes ribosome loss in aneuploid yeast cells. *Proc Natl Acad Sci U S A* **117**: 17031–17040.

Thorburn RR, Gonzalez C, Brar GA, Christen S, Carlile TM, Ingolia NT, Sauer U, Weissman JS, Amon A. 2013. Aneuploid yeast strains exhibit defects in cell growth and passage through START. *Mol Biol Cell* **24**: 1274–1289.

Tong AHY, Lesage G, Bader GD, Ding H, Xu H, Xin X, Young J, Berriz GF, Brost RL, Chang M, et al. 2004. Global Mapping of the Yeast Genetic Interaction Network. *Science* **303**: 808–813.

Torres EM, Sokolsky T, Tucker CM, Chan LY, Boselli M, Dunham MJ, Amon A. 2007. Effects of Aneuploidy on Cellular Physiology and Cell Division in Haploid Yeast. *Science* **317**: 916–924.

Trakala M, Aggarwal M, Sniffen C, Zasadil L, Carroll A, Ma D, Su XA, Wangsa D, Meyer A, Sieben CJ, et al. 2021. Clonal selection of stable aneuploidies in progenitor cells drives high-prevalence tumorigenesis. *Genes Dev* **35**: 1079–1092.

Voordeckers K, Kominek J, Das A, Espinosa-Cantú A, De Maeyer D, Arslan A, Van Pee M, Van Der Zande E, Meert W, Yang Y, et al. 2015. Adaptation to High Ethanol Reveals Complex Evolutionary Pathways. *PLOS Genet* **11**: e1005635.

Wangsa D, Braun R, Stuelten CH, Brown M, Bauer KM, Emons G, Weston LA, Hu Y, Yang HH, Vila-Casadesús M, et al. 2019. Induced Chromosomal Aneuploidy Results in Global and Consistent Deregulation of the Transcriptome of Cancer Cells. *Neoplasia* **21**: 721–729.

Watson EV, Lee JJ-K, Gulhan DC, Melloni GEM, Venev SV, Magesh RY, Frederick A, Chiba K, Wooten EC, Naxerova K, et al. 2024. Chromosome evolution screens recapitulate tissue-specific tumor aneuploidy patterns. *Nat Genet* **56**: 900–912.

Weaver BA, Cleveland DW. 2006. Does aneuploidy cause cancer? *Curr Opin Cell Biol* **18**: 658–667.

Yona AH, Manor YS, Herbst RH, Romano GH, Mitchell A, Kupiec M, Pilpel Y, Dahan O. 2012. Chromosomal duplication is a transient evolutionary solution to stress. *Proc Natl Acad Sci* **109**: 21010–21015.

Zhang K, Zhang L-J, Fang Y-H, Jin X-N, Qi L, Wu X-C, Zheng D-Q. 2016. Genomic structural variation contributes to phenotypic change of industrial bioethanol yeast *Saccharomyces cerevisiae*. *FEMS Yeast Res* **16**: fov118.

Zhou X, Hilk A, Solis NV, Scott N, Beach A, Soisangwan N, Billings CL, Burrack LS, Filler SG, Selmecki A. 2024. Single-cell detection of copy number changes reveals

dynamic mechanisms of adaptation to antifungals in Candida albicans. *Nat Microbiol* **9**: 2923–2938.

Figure 1

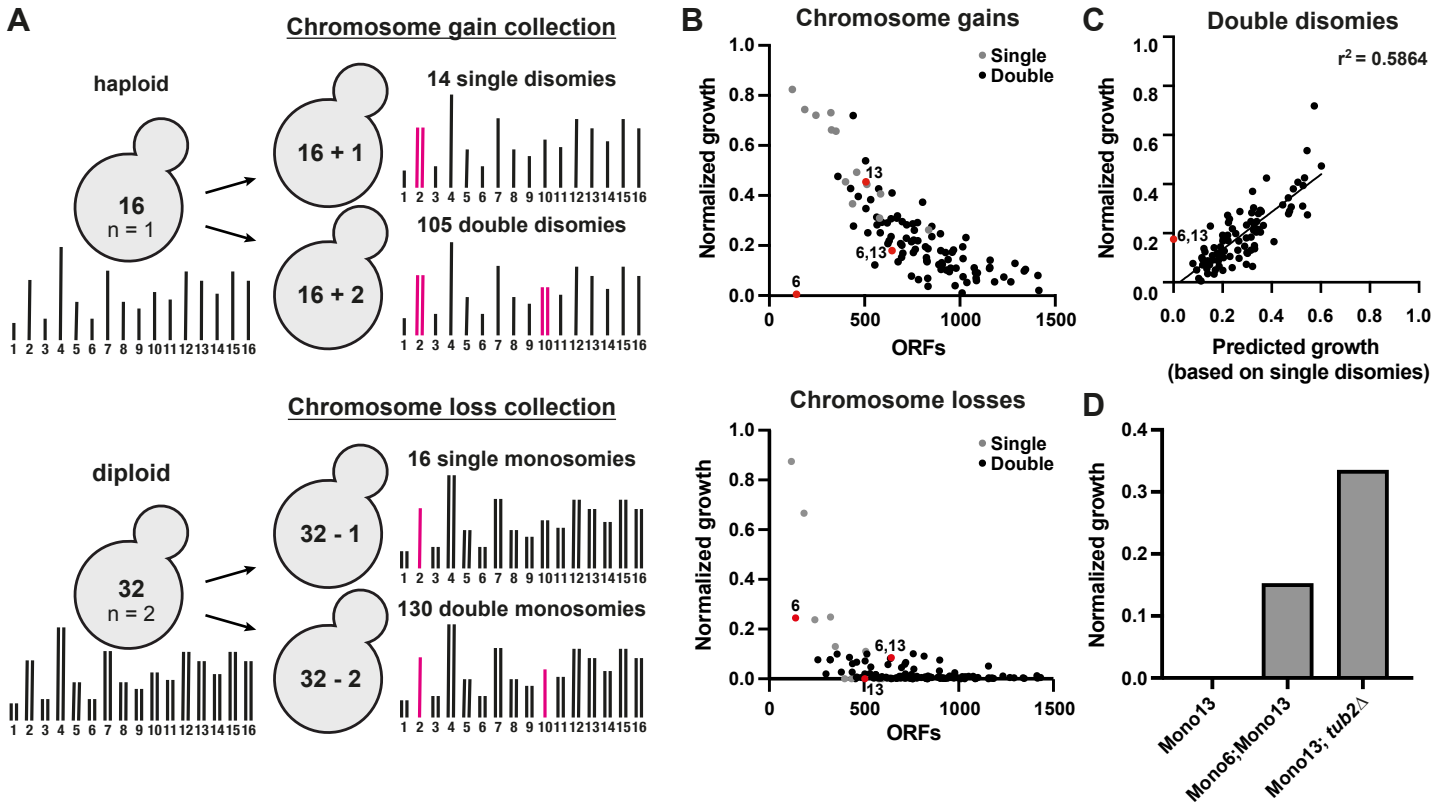

Figure 1: Strong genetic interactions between aneuploid chromosomes are rare
(A) Schematic overview of the chromosome gain and chromosome loss collections. (B) Quantified growth of the chromosome gain and chromosome loss collections. The averages of four independent high-throughput growth assays were normalized to WT. Colony intensities were quantified after 24h on YPAD plates for chromosome gains, and 72h on plates containing 5-Fluoroorotic Acid (5-FOA) for chromosome losses. Single disomies/monosomies are depicted in grey, double disomies/monosomies in black. (C) Correlation between growth of the double disomies and growth predictions based on the single disomies ($p < 0.0001$). Growth was predicted by calculating the product of single disomy growth. r^2 values are from simple linear regression and p-values are from *F*-tests. (D) Quantification of a serial dilution on 5-FOA plates after 72h normalized to a diploid WT.

Figure 2

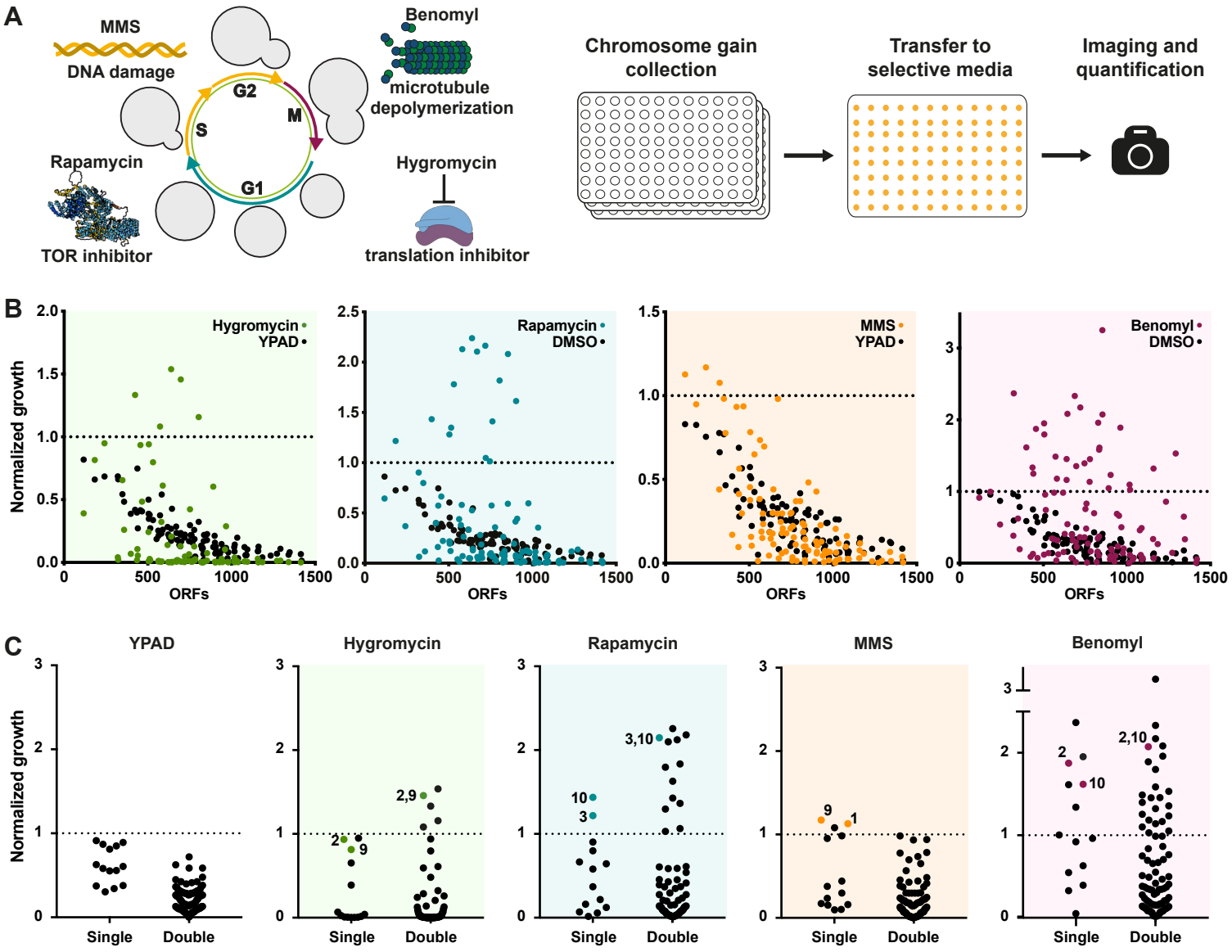

Figure 2: The strongest drug resistance phenotypes come from complex aneuploidy
(A) Schematic of the work-flow for plate-based high throughput growth assays under selective conditions. Cells were grown in liquid cultures before being transferred to condition specific agar plates. Images for colony intensities were taken after 24, 36, or 48h. (B) Averaged growth of two independent high-throughput growth assays. Control plates were quantified after 24h; hygromycin (40 µg/ml) and rapamycin (5 nM) plates after 48h; and MMS (0.02%) and benomyl (17.5 µg/ml) plates after 36h. All quantifications were normalized to a haploid WT. (C) Growth measurements of single disomies (Single) and double disomies (Double) across different treatments. The YPAD control is an average of YPAD and YPAD + DMSO plate growth. The dashed line indicates WT growth.

Figure 3

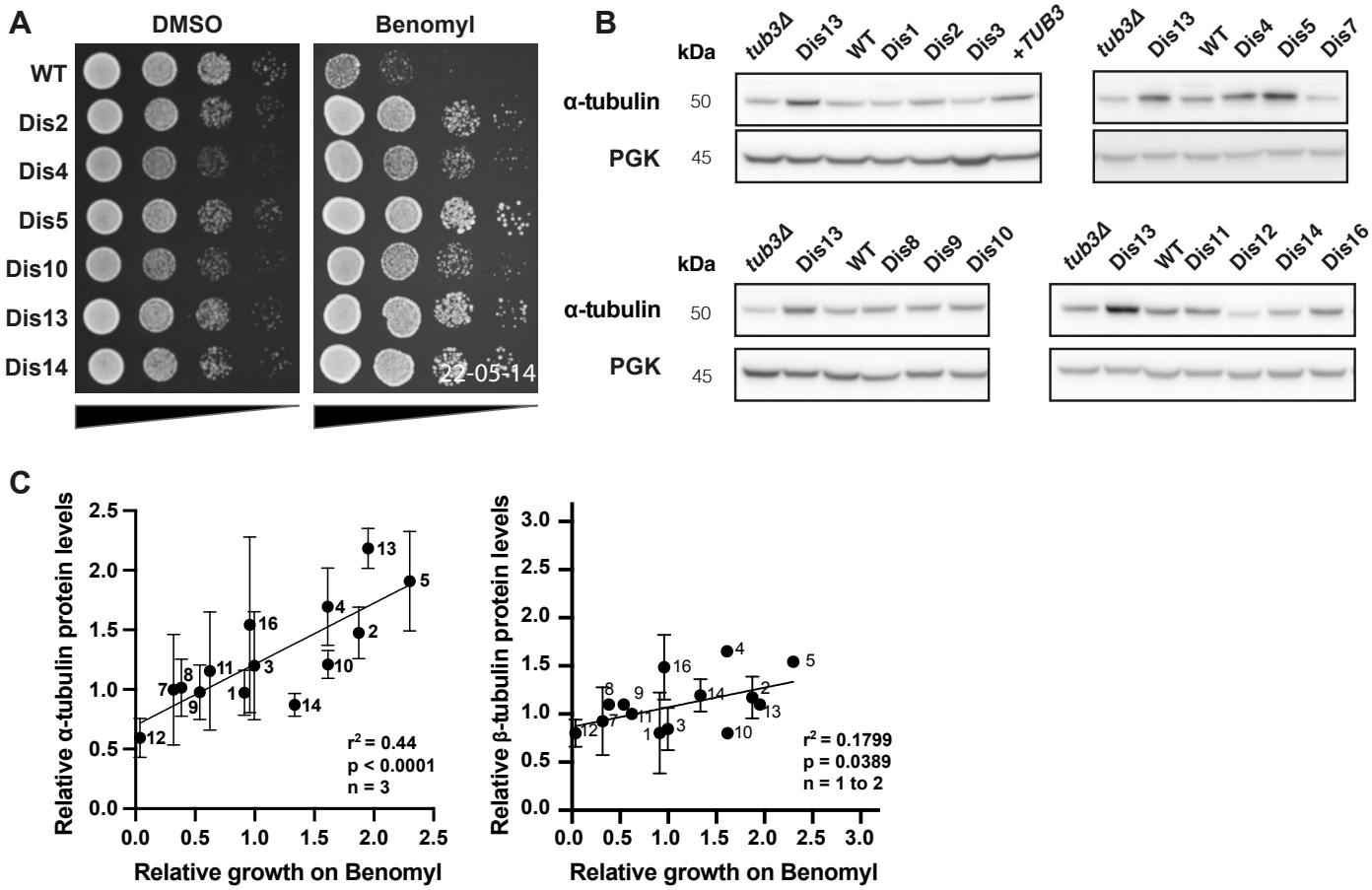

Figure 3: Benomyl resistance correlates with alpha-tubulin expression in aneuploid strains
(A) 10-fold serial dilution analysis of benomyl resistant single disomies on control (YPAD + DMSO, 24h) and treated (YPAD + 20 µg/ml benomyl, 48h) plates. (B) Western blot analysis of α-tubulin expression levels of single disomies. *Pgk1* is shown as a loading control. (C) Western blot quantifications of α-tubulin (n = 3) and β-tubulin (n = 1-2) expression levels for all single disomies. Strains were grown in YPAD and harvested in log-phase. Quantified bands were normalized to the Ponceau stained membrane and the haploid WT. Relative growth on benomyl denotes the average growth of single disomies from two independent high throughput colony size assays. r^2 values are from simple linear regression and p-values are from *F*-tests.

Figure 4

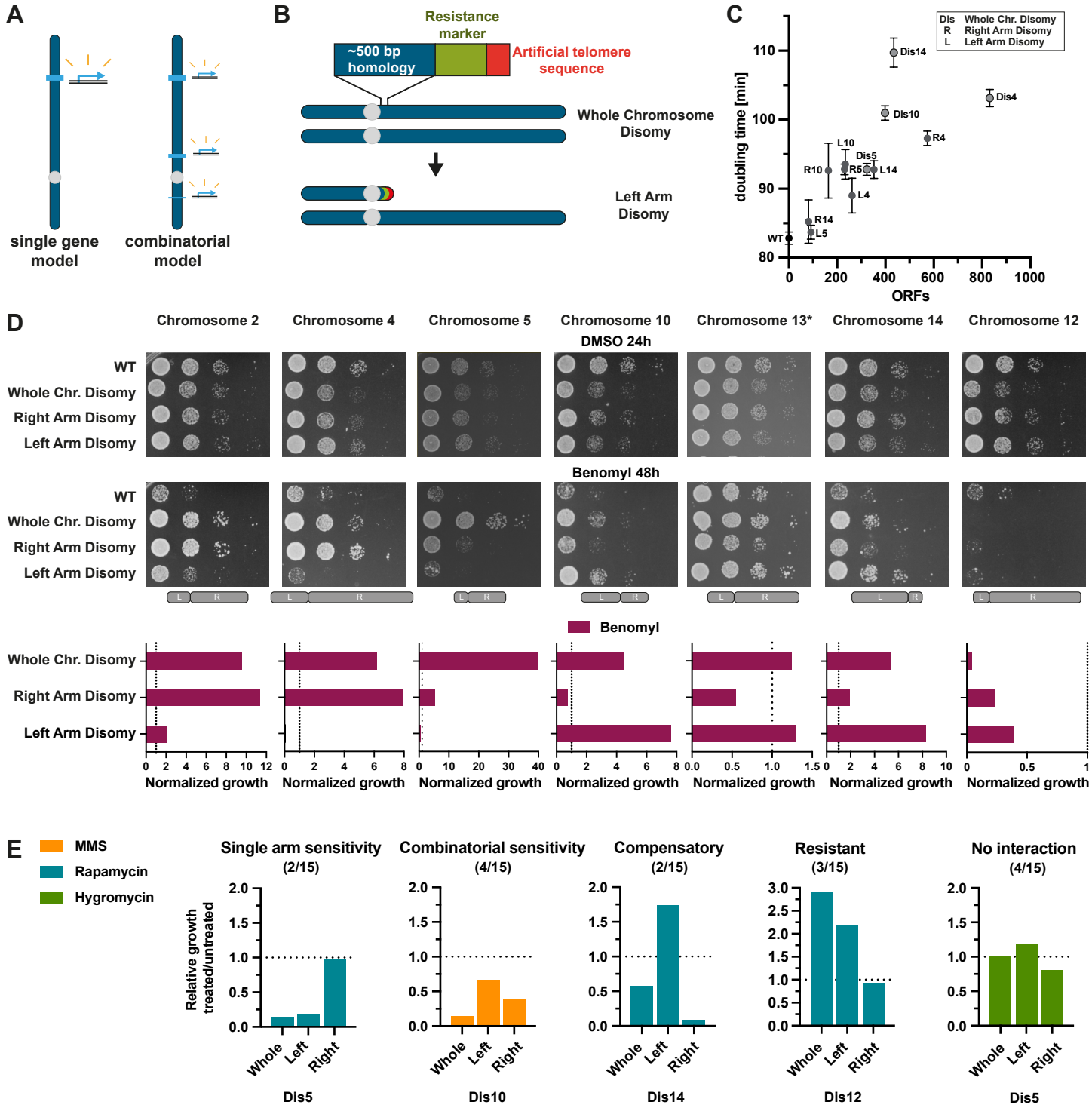
A
single gene model
combinatorial model
B
Resistance marker
~500 bp homology
Artificial telomere sequence
Whole Chromosome Disomy
Left Arm Disomy
C
Dis Whole Chr. Disomy
R Right Arm Disomy
L Left Arm Disomy
doubling time [min]
ORFs
Dis14
Dis4
Dis10
R4
L10
Dis5
R10
R5
L14
L4
R14
L5
WT
D
Chromosome 2
Chromosome 4
Chromosome 5
Chromosome 10
Chromosome 13*
Chromosome 14
Chromosome 12
DMSO 24h
Benomyl 48h
WT
Whole Chr. Disomy
Right Arm Disomy
Left Arm Disomy
Benomyl
Normalized growth
E
MMS
Rapamycin
Hygromycin
Single arm sensitivity (2/15)
Combinatorial sensitivity (4/15)
Compensatory (2/15)
Resistant (3/15)
No interaction (4/15)
Relative growth treated/untreated
Whole
Left
Right
Dis5
Dis10
Dis14
Dis12
Dis5

Figure 4: Identification of chromosome arms necessary for aneuploidy-based drug resistance.

(A) Schematic of two models for the genetic basis behind aneuploidy driven drug resistance. (B) Method of chromosome arm deletion. Chromosome arms are deleted by homologous recombination with a 500 bp homology sequence connected to a resistance marker and a telomeric seed sequence. (C) Doubling times of whole chromosome and single arm disomies for chromosomes 4, 5, 10 and 14. ORFs depict the remaining aneuploid ORFs after chromosome arm deletions. (D) 10-fold dilution series and quantification of whole chromosome and single arm disomies. Control plates (YPAD + DMSO) were imaged after 24h and treated plates (YPAD + 25 µg/ml benomyl) after 48h. * Indicates a lower benomyl concentration (20 µ/ml benomyl). The second dilution was quantified and normalized to WT, with the exceptions of chromosome 13 (third dilution) and chromosome 12 (first dilution). (E) Quantification of 10-fold serial dilutions treated with MMS (0.04 %), rapamycin (10 nM) or hygromycin (60 µg/ml). Relative growth was calculated as the ratio of normalized growth on treated plates (48h) to normalized growth on control plates (24h). Representative examples for single arm sensitivity, combinatorial sensitivity, compensatory sensitivity, resistance, and no interactions are shown. Images and quantifications of all 10-fold serial dilutions are depicted in Supplemental Fig. S4A, B.

Figure 5

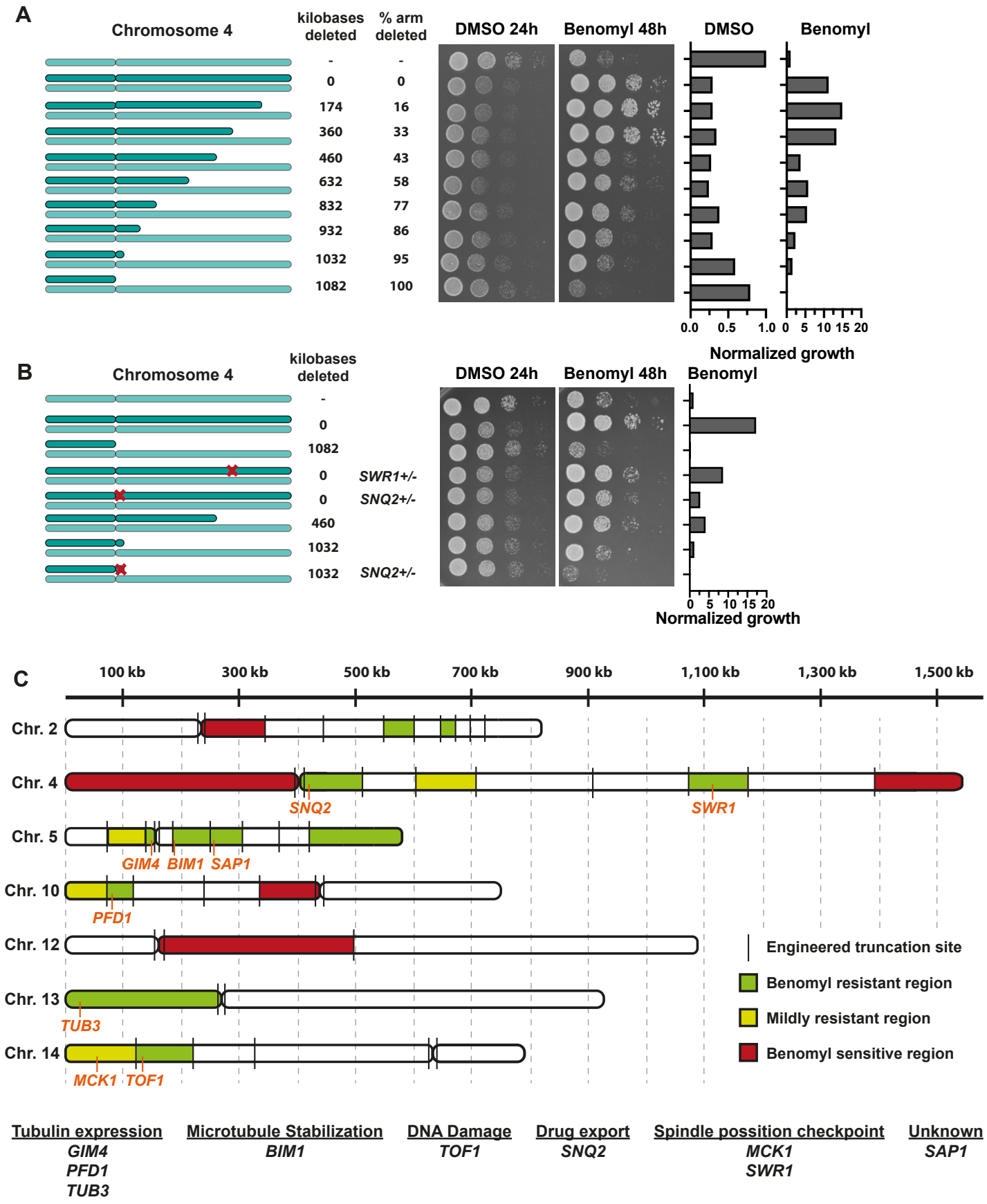
A
Chromosome 4
kilobases deleted
% arm deleted
DMSO 24h
Benomyl 48h
DMSO
Benomyl
-
0
174
360
460
632
832
932
1032
1082
0
16
33
43
58
77
86
95
100
0.0
0.5
1.0
0
5
10
15
20
Normalized growth
B
Chromosome 4
kilobases deleted
DMSO 24h
Benomyl 48h
Benomyl
-
0
1082
0
SWR1+/-
0
SNQ2+/-
460
1032
1032
SNQ2+/-
0
5
10
15
20
Normalized growth
C
100 kb
300 kb
500 kb
700 kb
900 kb
1,100 kb
1,300 kb
1,500 kb
Chr. 2
Chr. 4
SNQ2
SWR1
Chr. 5
GIM4
BIM1
SAP1
Chr. 10
PFD1
Chr. 12
Chr. 13
TUB3
Chr. 14
MCK1
TOF1
Engineered truncation site
Benomyl resistant region
Mildly resistant region
Benomyl sensitive region
Tubulin expression
GIM4
PFD1
TUB3
Microtubule Stabilization
BIM1
DNA Damage
TOF1
Drug export
SNQ2
Spindle possition checkpoint
MCK1
SWR1
Unknown
SAP1

Figure 5: Most aneuploidy-based drug resistance phenotypes come from the combined effects of multiple genes.
(A) 10-fold serial dilution and quantification of partial chromosome arm deletions of the right arm of chromosome 4. For control plates (YPAD + DMSO) the 3rd spot was quantified after 24h and for treated plates (YPAD + 25µg/ml benomyl) the 2nd and 3rd spots were quantified and averaged after 48h. Growth was normalized to a haploid WT. (B) 10-fold serial dilution and quantification of partial chromosome arm deletions and heterozygous deletions of genes contributing to benomyl resistance. For treated plates (YPAD + 25µg/l benomyl) the 2nd spot was quantified after 48h and normalized to the haploid wt. (C) Schematic depiction of benomyl resistant and sensitive chromosome regions. Identified resistance genes are indicated in orange at their approximate chromosomal location.

Figure 6

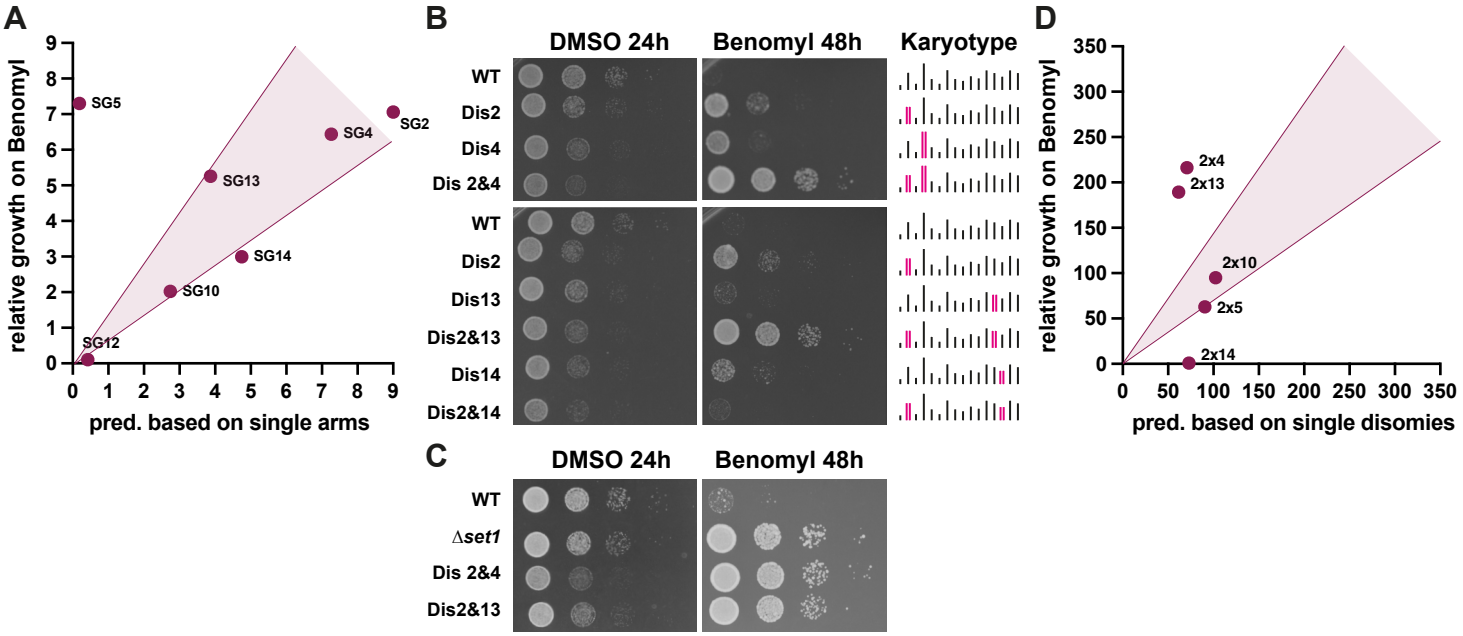

Figure 6: Synergistic effects contribute to the strongest aneuploidy phenotypes.
(A) Single disomy growth on benomyl compared to growth predictions based on single arm disomies. Growth was quantified from 10-fold serial dilutions in Figure 4D. The area highlighted in magenta indicates additive genetic interactions (+/-30% of predicted growth). Disomies that fall below this threshold are considered a negative synergistic interaction and those above are considered a positive synergistic interaction. (B) 10-fold serial dilution of single and double disomies. Control plates (YPAD + DMSO) were imaged after 24h and treated plates (YPAD + 30 µg/ml benomyl) after 48h. (C) 10-fold serial dilutions of benomyl resistant *set1*Δ haploid and two synergistically interacting double disomies (2&4, 2&13). Benomyl plates contained 30 µg/ml benomyl. (D) Quantification of the 10-fold serial dilutions of the double disomies on plates with 30 µg/ml benomyl compared to predicted growth based on the additive resistance of the single disomies (for images, see Sup. Figure 8A). Combinations in the highlighted area (magenta) are additive genetic interactions (+/-30% of predicted growth). Disomy combinations that fall below this threshold are considered a negative synergistic interaction and those above are considered a positive synergistic interaction.